PHOTONICS Research

Investigation of nonlinear optical properties of rhenium diselenide and its application as a femtosecond mode-locker

Jinho Lee, Kyungtaek Lee, Suhyoung Kwon, Bumsoo Shin, and Ju Han Lee*

School of Electrical and Computer Engineering, University of Seoul, Seoul 02504, South Korea
*Corresponding author: j.h.lee@ieee.org

Received 18 April 2019; revised 14 June 2019; accepted 27 June 2019; posted 28 June 2019 (Doc. ID 364728); published 9 August 2019

We investigated the nonlinear optical properties of $ReSe_2$. First, we measured the nonlinear absorption coefficient and the nonlinear refractive index of a $ReSe_2$ thin film using open-aperture (OA) and closed-aperture (CA) Z-scan techniques. $ReSe_2$ was shown to possess both saturable absorption and self-defocusing properties. The nonlinear absorption coefficient of $ReSe_2$ was measured to be $-(5.67 \pm 0.35) \times 10^3$ cm/GW, and its nonlinear refractive index was $-(2.81 \pm 0.13) \times 10^{-2}$ cm^2/GW at 1560 nm. Next, a fiberized saturable absorber (SA) based on $ReSe_2$ was fabricated with a side-polished fiber platform and was tested as an ultrafast mode-locker capable of producing femtosecond pulses operating at a wavelength of 1560 nm. The estimated modulation depth and saturation power are ~3.9% and ~42 W, respectively, for the transverse electric mode, while they are ~2.4% and ~53 W for the transverse magnetic mode. Using the prepared SA, stable soliton pulses with a temporal width of ~862 fs were produced from an erbium-doped fiber ring cavity. To the best of the authors' knowledge, this is the first demonstration of using a $ReSe_2$-based SA for femtosecond mode-locked pulse generation.

https://doi.org/10.1364/PRJ.7.000984

1. INTRODUCTION

Optical materials with nonlinear properties have always been important for the field of nonlinear optics (NLO) since they can be used for practical applications such as optical switching, mode-locking, and optical limiting [1–9]. Optical nonlinearity means that the physical parameters of a material, such as absorptivity and refractive index, are electric field intensity dependent. In the past several decades, a number of materials have been found to possess significant nonlinear optical properties [10–12]. In particular, nanostructured materials have recently been a focus of research since they provide a flexible platform for the implementation of various functional electronic or photonic devices that are difficult to realize with traditional bulk-structured material platforms. Nanostructured nonlinear optical materials include carbon nanotubes (CNTs) [13,14], graphene [15–17], graphene oxide (GO) [18,19], topological insulators (TIs) [20–25], transition-metal dichalcogenides (TMDCs) [6,8,26–45], black phosphorus (BPs) [46–48], gold nanoparticles [49,50], skutterudites [51,52], MXenes [53,54], and transition-metal monochalcogenides (TMMCs) [55]. It should be noted that nanostructured materials do not imply two-dimensional (2D) materials even if 2D materials are included in the material structure.

One family of recently discovered nanostructured materials consists of TMDCs [56]. TMDCs are materials with a formula of MX_2, where M is a transition metal element (e.g., Mo, W, and Nb) and X is a chalcogen (e.g., S, Se, or Te). TMDCs have a layered $X-M-X$ structure, wherein a layer of the transition metal atom is sandwiched between two layers of chalcogen atoms. The adjacent layers are weakly bonded together by van der Waals forces, and therefore thin sheets can be easily exfoliated from the bulk material. A number of investigations of the nonlinear optical properties of TMDCs have been conducted thus far, and their utilization in optical devices has been extensively demonstrated. For example, Zhang *et al.* reported the saturable absorption property of molybdenum disulfide (MoS_2) for the first time [6], to the best of our knowledge. Two-photon absorption (TPA) of tungsten disulfide (WS_2) and MoS_2 was investigated by Zhang *et al.* [57]. The second and third-order optical susceptibilities of MoS_2 were investigated by a number of research groups [58–60].

Rhenium diselenide ($ReSe_2$) is a rhenium-based TMDC. Compared to commonly known molybdenum- or tungsten-based TMDCs, rhenium-based TMDCs such as ReS_2 and $ReSe_2$ have attracted less technical attention until recently, even though they possess electronic or optical properties comparable to the aforementioned common TMDCs [61–63]. Very recently, quite a few investigations of the nonlinear optical properties of ReS_2 and $ReSe_2$ have been conducted [34–42]. In particular, most of the investigations of $ReSe_2$ have focused

on saturable absorption. For example, Du *et al.* reported saturable absorption properties of $ReSe_2$ for the first time, to the best of our knowledge, and demonstrated a $ReSe_2$-based saturable absorber (SA) for a *Q*-switched fiber laser [39]. Li *et al.* systematically investigated nonlinear saturable absorption properties of $ReSe_2$ at 1030 and 515 nm using an open-aperture (OA) Z-scan technique and demonstrated its use for picosecond mode-locking of a 1064 nm waveguide laser [40]. Investigations regarding $ReSe_2$-based SAs have also been conducted by Li *et al.* [41,42].

In this paper, we report a detailed investigation of the nonlinear optical properties of $ReSe_2$ at a wavelength of 1560 nm. This investigation was conducted with three-dimensional (3D) structured $ReSe_2$, as opposed to 2D structured. First, we show experimental measurements of the nonlinear absorption coefficient and the nonlinear refractive index of a thin $ReSe_2$ film with an OA and closed-aperture (CA) Z-scan technique. Note that unlike our measurements, the Z-scan measurement of $ReSe_2$ by Li *et al.* was based on an OA technique to obtain limited information about saturable absorption properties at 1030 and 515 nm [40]. Our measurements are conducted with a femtosecond fiber laser at a wavelength of 1560 nm and show that $ReSe_2$ has both saturable absorption and self-defocusing properties. Next, a fiberized SA based on $ReSe_2$ is fabricated with a side-polished fiber platform. Finally, the fabricated SA is tested as an ultrafast mode-locker and was found to be capable of producing femtosecond pulses operating at a wavelength of 1560 nm. To the best of the author's knowledge, there have been no previous reports of $ReSe_2$-based SAs for use in the femtosecond mode-locking of a laser.

2. FABRICATION AND CHARACTERIZATION OF A $ReSe_2$-BASED THIN FILM

To fabricate a $ReSe_2$ thin film, $ReSe_2$ bulk flakes (99.99%, HQ graphene) were used as a starting material. Nanometer- or micrometer-sized $ReSe_2$ particles were first obtained using bath-type ultrasonification in 10 mL of distilled water for 16 h. Note that no additional centrifugation step for elimination of large agglomerates was conducted in our case, since our target particles were not nano-sized particles. Figure 1(a) shows scanning electron microscopy (SEM) image of the obtained $ReSe_2$ particles. Their sizes are observed to vary from tens of nanometers to around 2 μm. An energy-dispersive spectroscopy (EDS) measurement was also conducted, as shown in Fig. 1(b). For the EDS measurement, a small amount of solution containing $ReSe_2$ particles was dropped and dried on top of a glass slide. The two strong peaks observed at 1.85 keV and 1.4 keV are associated with Re (M_α) and Se (L_α) [64], and the atomic ratio between Re and Se was approximately 1:2.

To form a thin film, polyvinyl alcohol (PVA) was mixed with the prepared $ReSe_2$ solution. The concentration of $ReSe_2$ in the $ReSe_2$/PVA composite was ~1 $mg \cdot mL^{-1}$. An atomic force microscope (AFM) image of our prepared $ReSe_2$ thin film has been measured, as shown in Fig. 2. The thickness of the prepared $ReSe_2$ particles within the target range was measured to be ~450 nm. However, note that the thickness of prepared $ReSe_2$ particles was random since no centrifugation process was used after ultrasonication. It was thus impossible to obtain a reasonable average thickness and layer number from a limited number of AFM-measured values.

To analyze the stoichiometry of the $ReSe_2$/PVA thin film, X-ray photoelectron spectroscopy (XPS) measurements were performed. High-resolution spectra of the Re 4f and Se 3d region are shown in Figs. 3(a) and 3(b), respectively. The two peaks of Re $4f_{7/2}$ and Re $4_{5/2}$ at ~41.6 and ~44 eV are consistent with previously reported results [64,65]. Two peaks at 54.6 and ~55.6 eV in the Se-3d region of Fig. 3(b) are consistent with the peaks of Se $3d_{5/2}$ and Se $3d_{3/2}$ [64,65]. The measured high-resolution spectrum for the C 1s region confirms the existence of CH_2 and CH–OH groups in the PVA [66]. The peaks centered at the binding energies of ~284 eV, ~286 eV, ~288.7 eV in the C 1s region can be attributed to CH_2, CH–OH, and C=O groups, respectively [66,67].

Next, we measured the Raman spectrum of the $ReSe_2$/PVA thin film at 532 nm (InVia Raman Microscope, Renishaw) [Fig. 4(a)]. Many small peaks were observed due to the complex lattice vibration and low symmetry of $ReSe_2$ used [41,42,64,65,68–70]. Three main Raman peaks at ~124, ~159, and ~173 cm^{-1} indicate in-plane (E_g) and out-of-plane (A_g) vibrational modes [41,42,64,65,68–70]. Figure 4(b) shows the measured linear optical absorption of the $ReSe_2$/PVA composite film over a spectral range of 1000–1800 nm, which was measured using a spectrophotometer

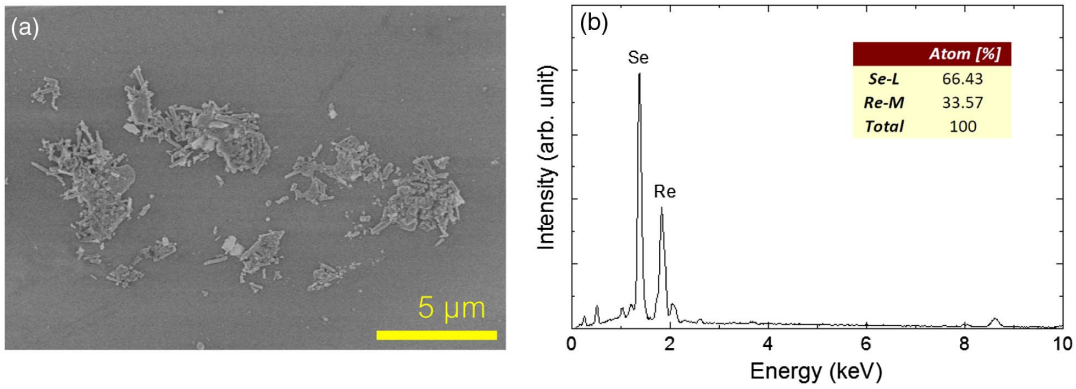

Fig. 1. (a) SEM image and (b) EDS spectrum of the prepared $ReSe_2$ particles.

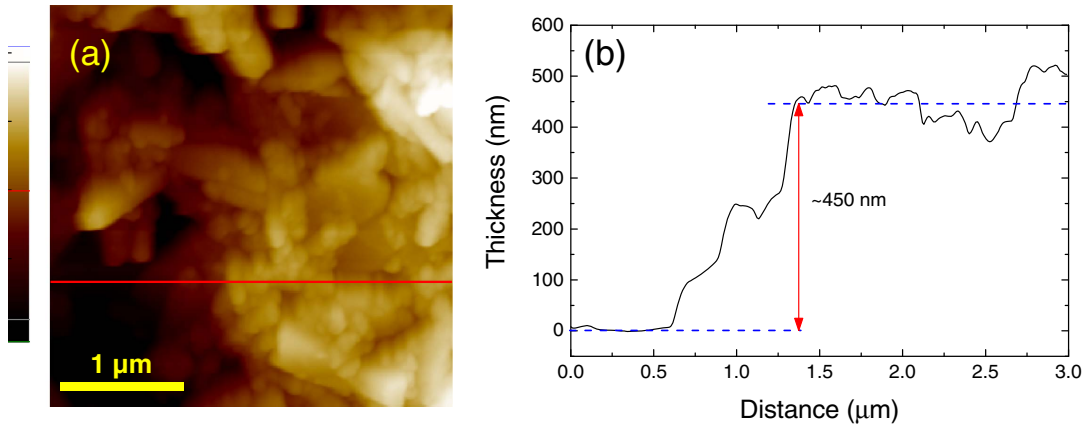

Fig. 2. (a) AFM image and (b) line profile of the $ReSe_2$ thin film.

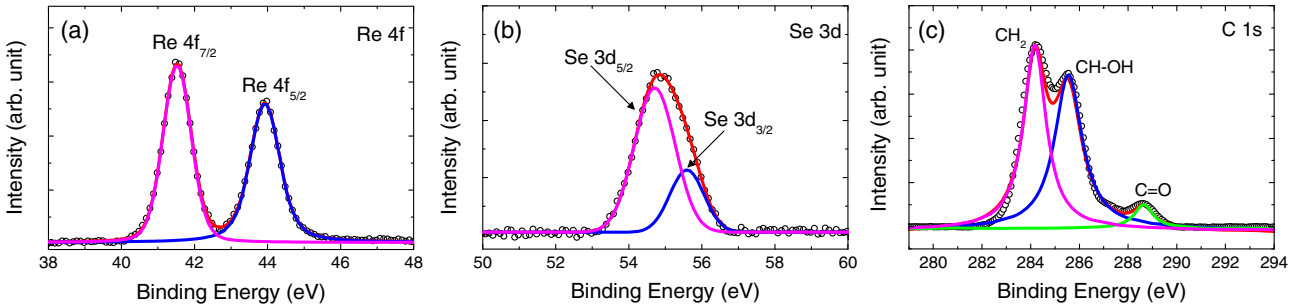

Fig. 3. XPS spectra of the prepared $ReSe_2$/PVA thin film in the (a) Re 4f region, (b) Se 3d region, and (c) C 1s region.

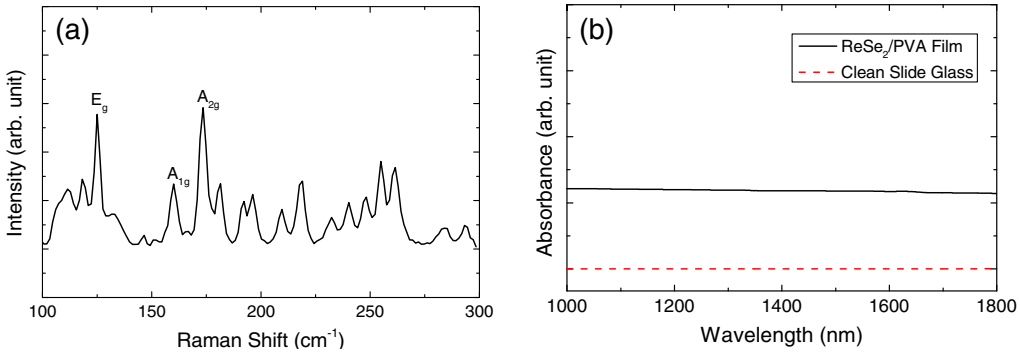

Fig. 4. (a) Measured Raman spectrum of the $ReSe_2$/PVA thin film. (b) Linear optical absorption spectrum of the $ReSe_2$/PVA composite.

(UV-3600PLUS, Shimadzu). For the measurement, the $ReSe_2$/PVA composite solution was deposited onto a glass slide. A broad absorption band of the prepared $ReSe_2$/PVA composite was clearly observed, which included absorption in the 1.5 μm wavelength band.

It was reported that the energy bandgap of bulk $ReSe_2$ is around 0.995 eV (1246 nm), while that of a $ReSe_2$ monolayer is 1.24 eV (1000 nm) [70,71]. From the perspective of the energy bandgap, it should thus be impossible to observe photon absorption from the $ReSe_2$ particles at wavelengths above 1246 nm. However, as shown in Fig. 4(b), the optical absorption of the prepared $ReSe_2$/PVA film was clearly observed in the 1.5 μm wavelength region. Such absorption behavior could be attributed to Re and Se atomic defects [40]. As mentioned in Ref. [40], the atomic defects could reduce the energy bandgap of $ReSe_2$, allowing for broadband photon absorption irrespective of the energy bandgap of the pristine material. In fact, sub-bandgap absorption has been previously reported in other

TMDC materials. It is well-known that the broken symmetry and unsatisfied bonds between M and X atoms at edges can modify the electronic structures of TMDCs [72].

3. Z-SCAN MEASUREMENT FOR A $ReSe_2$-BASED THIN FILM

The measurements for the nonlinear optical response of the $ReSe_2$ particles were carried out by using the OA and CA Z-scan techniques [73]. The experimental setup is shown in Fig. 5(a). A homemade mode-locked fiber laser with a repetition rate of 22.26 MHz and a pulse width of 300 fs at a wavelength of 1560 nm was used as an input source. To obtain the nonlinear absorption coefficient, an OA Z-scan measurement was first performed with the aperture fully opened ($S = 1$). The beam was focused through a plano-convex lens to obtain a peak intensity of about 50 MW/cm^2. The position of the sample was changed from $z = -15$ mm to $z = 15$ mm with a step size of 0.5 mm. The spot size was estimated from the obtained curve, which was approximately 22 μm at the focal point. The average thickness of the prepared $ReSe_2$/PVA film was approximately 9 μm. The formed $ReSe_2$/PVA thin film had a circular shape with a diameter of ~10 mm, which is much larger than the beam waist of ~22 μm. The Z-scan setup was calibrated considering the effect of the substrate.

As shown in Fig. 5(b), the change of the transmittance of the sample was measured with a photodiode sensor; the normalized values of the measured data were plotted against the z position and fitted with the following formula [73,74]:

$$T(z) = \sum_{n=0}^{\infty} (-\beta I_0 L_{\text{eff}})^n/(1 + z^2/z_0^2)^n(n+1)^{3/2} \approx 1 - \beta I_0 L_{\text{eff}}/2^{3/2}(1 + z^2/z_0^2), \quad (1)$$

where $T(z)$ is the normalized transmittance, β is the nonlinear absorption coefficient, I_0 is the peak on-axis intensity at the focus, L_{eff} is the effective length, z is the position of the sample, and z_0 is the Rayleigh length.

To determine the sign and magnitude of the nonlinear refractive index of the $ReSe_2$ sample, a CA Z-scan measurement was subsequently conducted, while the aperture at the far field was kept closed ($S \sim 0.7$). In the CA Z-scan measurement, the transmitted beam is sensitive to both nonlinear absorption and nonlinear refraction. By dividing the normalized results of a CA Z scan by those of an OA Z scan, we can distinguish the nonlinear refraction from the nonlinear absorption [73]. The normalized values of the measured data were plotted against the z position and fitted with the following formula [75]:

$$T(z) = \frac{1}{1 - \frac{4z/z_0}{(1+z^2/z_0^2)^2}\Delta\Phi + \frac{4}{(1+z^2/z_0^2)^3}\Delta\Phi^2}, \quad (2)$$

where $\Delta\Phi = 2\pi n_2 I_0 L_{\text{eff}}/\lambda$ is the phase change, n_2 is the nonlinear refractive index, $L_{\text{eff}} = (1 - e^{-\alpha_0 L})/\alpha_0$ is the effective thickness of the sample, α_0 is the linear absorption coefficient, L is the thickness of the sample, $z_0 = \pi\omega_0^2/\lambda$ is the Rayleigh length, ω_0 is the beam waist, λ is the wavelength, and I_0 is the intensity at the focusing point. The measured nonlinear absorption coefficient of the $ReSe_2$/PVA film was $-(5.67 \pm 0.35) \times 10^3$ cm/GW, and its nonlinear refractive index was $-(2.81 \pm 0.13) \times 10^{-2}$ cm^2/GW.

The curves in Fig. 5(b) show the nonlinear saturable absorption and self-defocusing behaviors of the $ReSe_2$ film at a wavelength of 1560 nm. Considering the bandgap of the pristine $ReSe_2$ [70,71], the $ReSe_2$ was supposed to exhibit TPA at 1560 nm; however, no TPA was observed in our $ReSe_2$ sample [76,77]. On the other hand, our measurement results revealed that $ReSe_2$ possesses a saturable absorption property, even for incident photons with energies lower than its bulk bandgap energy. The nonlinear saturable absorption of $ReSe_2$ could be attributed to a defect-driven bandgap decrease or edge state absorption [72]. Note that TMDC materials with bandgap energies larger than the incident photon energy are known to exhibit such a saturable absorption behavior in the 1550 nm wavelength region [76,77]. Table 1 compares the Z-scan-measured nonlinear optical parameters of a variety of TMDCs with those of $ReSe_2$. Note that the previous measurements for nonlinear absorption coefficients and the nonlinear refractive indices of TMDCs were conducted at wavelengths of 515, 800, 1030, or 1064 nm. Since our measurements were conducted at 1560 nm, it is impossible to directly compare our measured nonlinear optical parameters of $ReSe_2$ to those of the other MDCs. It is believed that $ReSe_2$ has nonlinear optical properties comparable to various TMDCs.

In this experiment, we have not observed TPA in our prepared $ReSe_2$/PVA film. This could be attributed to the fact that our used pulse laser for the Z-scan measurements might not have a peak power high enough to induce TPA. Regarding the effect of a large nonlinear absorption coefficient β on the mode-locking performance, we believe that a large nonlinear

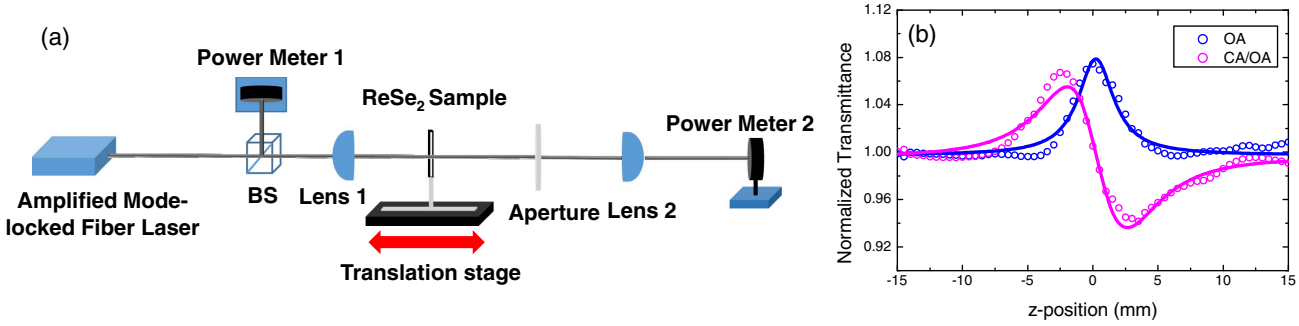

Fig. 5. (a) Schematic diagram of the Z-scan measurement setup at 1560 nm. BS: beam splitter. (b) Z-scan results for the $ReSe_2$ film using open-aperture (OA) and closed-aperture (CA) Z scan.

Table 1. Comparison of Nonlinear Optical Parameters for a Range of TMDCs that Were Measured with the Z-Scan Technique

Sample	NLO Response	λ (nm)	α_0 (cm^{-1})	β (cm/GW)	n_2 (cm^2/GW)	Reference
WS_2	SA[a]	800	8.88 nm^{-1}	$-(3.7 \pm 0.28) \times 10^5$	8.1 ± 0.41	[78]
WS_2	SA	1064	NA[c]	$-(5.1 \pm 0.26)$	$(5.83 \pm 0.18) \times 10^{-2}$	[79]
MoS_2	SA	1064	NA	$-(3.8 \pm 0.59)$	$(1.88 \pm 0.48) \times 10^{-3}$	[79]
WSe_2	TPA[b]	1064	NA	(1.9 ± 0.57)	$-(2.4 \pm 1.23)$	[79]
$Mo_{0.5}W_{0.5}S_2$	TPA	1064	NA	(1.91 ± 0.78)	$-(8.73 \pm 1.47) \times 10^{-2}$	[79]
WS_2 (1–3L)	TPA	1030	7.17×10^5	$(1.0 \pm 0.8) \times 10^4$	NA	[57]
WS_2 (18–20L)	TPA	1030	5.98×10^5	$(3.28 \pm 0.11) \times 10^3$	NA	[57]
WS_2 (39–41L)	TPA	1030	8.57×10^5	$(2.75 \pm 0.11) \times 10^3$	NA	[57]
MoS_2 (25–27L)	TPA	1030	3.90×10^4	66 ± 4	NA	[57]
MoS_2 (72–74L)	SA	1030	1.89×10^5	-250 ± 50	NA	[57]
WS_2 (1–3L)	TPA	800	1.08×10^6	525 ± 205	NA	[57]
WS_2 (18–20L)	SA	800	7.22×10^5	-397 ± 40	NA	[57]
MoS_2 (25–27L)	TPA	800	6.24×10^4	11.4 ± 4.3	NA	[57]
WS_2 (1–3L)	SA	515	5.18×10^4	$-(2.9 \pm 1.0) \times 10^4$	NA	[57]
$ReSe_2$	SA	1560	0.25×10^3	$-(5.67 \pm 0.35) \times 10^3$	$-(2.81 \pm 0.13) \times 10^{-2}$	This work

[a]SA, saturable absorption.
[b]TPA, two photon absorption.
[c]NA, not available.

absorption coefficient β of a nonlinear optical material is associated with a large modulation depth of the material-based SA. Note that the use of an SA with a larger modulation depth is known to increase the mode-locking stability as well as to reduce the mode-locked pulse width [80,81]. The relaxation time measurement of the $ReSe_2$ sample was not conducted since no pump–probe spectroscopy setup was available in our laboratory.

4. FABRICATION OF A $ReSe_2$-BASED FIBERIZED SATURABLE ABSORBER

Next, we fabricated a fiberized SA that can be used for ultrafast mode-locking based on $ReSe_2$. A side-polished fiber was employed as a platform. The side-polished fiber was prepared through the polishing of one side of an SMF-28 fiber, which was fixed onto the V groove of a glass slide. The cross-sectional structure of the prepared SA is shown in Fig. 6(a). The insertion loss and polarization-dependent loss (PDL) of the prepared side-polished fiber were ~0.8 dB and ~0.05 dB at 1560 nm, respectively. The physical distance of the flat side to the edge of the fiber core was of ~7 μm, and the polishing length was ~2.5 mm. The $ReSe_2$/PVA solution was deposited onto the flat side of the side-polished fiber using the solution-drop method and then dried at room temperature for 24 h. The insertion loss and PDL of the $ReSe_2$/PVA-deposited side-polished fiber were ~2.9 dB and ~1.6 dB, respectively.

Nonlinear transmission curves of the $ReSe_2$/PVA-based SA were measured as a function of the incident peak power of the input pulses for transverse electric (TE) and transverse magnetic (TM) modes, respectively. For this measurement, we used a mode-locked, 1.56 μm fiber laser with a temporal width of ~680 fs at a repetition rate of ~22.26 MHz, and the measurement setup is shown in Fig. 6(b). Since our SA had a non-negligible PDL of ~1.6 dB, a polarization controller (PC) was incorporated into the measurement setup. It was straightforward to distinguish the TE and TM modes by measuring the output power while the PC was adjusted. A variable optical attenuator (VOA) was used to adjust the optical power of the mode-locked pulses. A 50:50 coupler was used to split the mode-locked pulses into two ports. One of the two ports was connected to the prepared $ReSe_2$/PVA-based SA, while the other was directly connected to a power meter to monitor the input beam power on the prepared SA. Another power meter was used to monitor the output power from the $ReSe_2$/PVA-based SA for comparison with the input power. Figure 7 shows the nonlinear transmission curves for the TE and TM modes fitted to the following equation [82]:

$$T(I) = 1 - \Delta T \cdot \exp\left(\frac{-I}{I_{\text{sat}}}\right) - T_{\text{ns}}, \tag{3}$$

where T is the transmission, ΔT is the modulation depth, I is the incident pulse energy, I_{sat} is the saturation energy, and

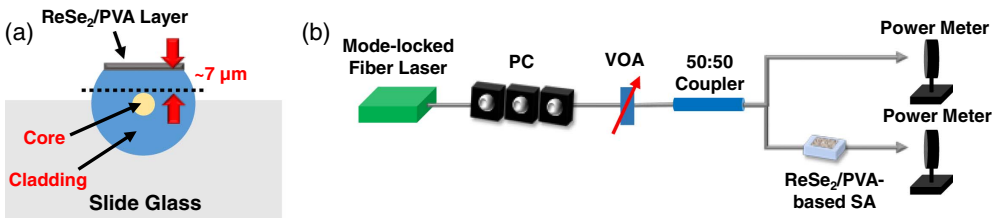

Fig. 6. (a) Schematic of our prepared $ReSe_2$/PVA-deposited side-polished fiber. (b) Measurement setup for nonlinear transmission curves of the $ReSe_2$/PVA-based SA at 1560 nm.

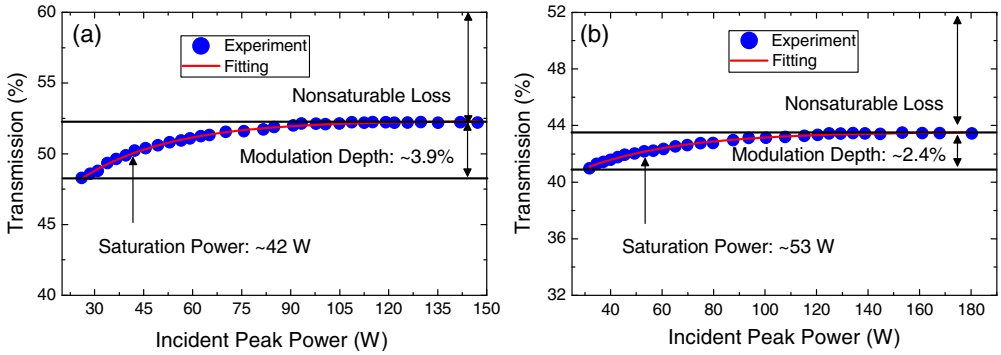

Fig. 7. Nonlinear transmission curves of the $ReSe_2$/PVA-deposited side-polished fiber: (a) the transverse electric (TE) mode and (b) the transverse magnetic (TM) mode.

T_{ns} is the nonsaturable loss. The estimated modulation depth and saturation power for the TE mode are ~3.9% and ~42 W, respectively, while they are ~2.4% and ~53 W, respectively, for the TM mode. Due to the asymmetric structure of our prepared $ReSe_2$/PVA-deposited side-polished fiber, the TE and TM modes have different interaction strengths between the $ReSe_2$/PVA film and oscillating beam. This is the reason why the TE and TM modes exhibit different saturable absorption properties. Regarding the main mode for the actual mode-locking, we believe that the TE mode would play a key role in our laser setup since the TE mode experiences less insertion loss. It is believed that the modulation depth level is high enough to induce soliton mode-locking in the fiberized laser cavity with proper anomalous dispersion [81].

In order to measure the damage threshold of the proposed $ReSe_2$/PVA-based SA, we have launched a 1550 nm continuous-wave amplified laser beam of 1 W power into it. However, we have not observed any substantial damage of the device within the optical power level. Therefore, we believe that the damage threshold of the prepared $ReSe_2$/PVA-based SA must be larger than 1 W. However, it was impossible to measure the precise value due to the limited availability of a high-power laser in our laboratory.

5. MODE-LOCKING PERFORMANCE MEASUREMENTS

The experimental schematic of our passively mode-locked fiber laser is shown in Fig. 8. The gain medium is a 2.3-m-long erbium-doped fiber (EDF) with peak absorption of ~20 dB/m at a wavelength of 1530 nm. A 980 nm pump laser diode was used as the pump source that was inserted into the gain medium through a 980/1550 nm wavelength division multiplexer (WDM). The polarization-independent isolator was used to force unidirectional light propagation. The mode-locked laser output was extracted from the ring cavity using the 10% port of a 90:10 coupler. A PC was used to optimize the polarization state of the oscillating beam within the laser cavity. The $ReSe_2$/PVA-deposited side-polished fiber was placed after the PC.

Stable mode-locked pulses were readily obtained when the pump power was set to ~19.6 mW, with the PC properly adjusted. The average output power was measured to be ~0.5 mW. The main factor limiting the output power is the unoptimized cavity configuration. To optimize the laser cavity to produce higher average output power, we tried to reduce the insertion loss of the prepared SA as well as to change the output coupler. To control the insertion loss of the prepared SA, we need to optimize the side-polished fiber in terms of its polishing depth, interaction length, and the concentration of the solution. Such work to enhance the laser performance is reserved for future work. Figure 9(a) shows the measured optical spectrum of the mode-locked pulses. Kelly sidebands were clearly observed, indicating that the fiber laser was operating in the soliton regime [83]. The center wavelength and 3 dB bandwidth of the pulses were measured to be ~1561.2 nm and ~3.4 nm, respectively. Figure 9(b) shows the measured oscilloscope trace of the output pulses with a 16 GHz real time oscilloscope combined with an 11 GHz photodetector. The inset of Fig. 9(b) shows a magnified view of a single output pulse. The temporal period of the output pulse is ~66.8 ns, which corresponds to the fundamental repetition rate of ~14.97 MHz.

Next, an autocorrelation measurement was performed using a TPA-based autocorrelator. Figure 10(a) shows the measured autocorrelation trace of the output pulses with a hyperbolic secant-squared fitting curve. The estimated temporal width of the output pulses is ~862 fs. Considering the 3 dB bandwidth of ~3.4 nm, the estimated time-bandwidth product is ~0.361, indicating that the output pulses are slightly chirped. The electrical spectrum was measured to confirm the stability of the output pulses, as shown in Fig. 10(b). A strong signal peak with an electrical signal-to-noise ratio (SNR) of ~65 dB was obtained at a fundamental repetition rate of ~14.97 MHz. The inset of Fig. 10(b) shows the electrical spectrum with a 1 GHz frequency span. Strong harmonic signals were clearly observed, strongly indicating that the output pulses are stable mode-locked pulses.

The solution dropping is a simple method to form a thin film on a substrate by dropping and drying a small amount of solution. However, it is difficult to control the uniformity of the film thickness using this method. The saturable absorption performance of our prepared SA was observed to change in some degree sample by sample. However, the output performance of our mode-locked laser was not observed to

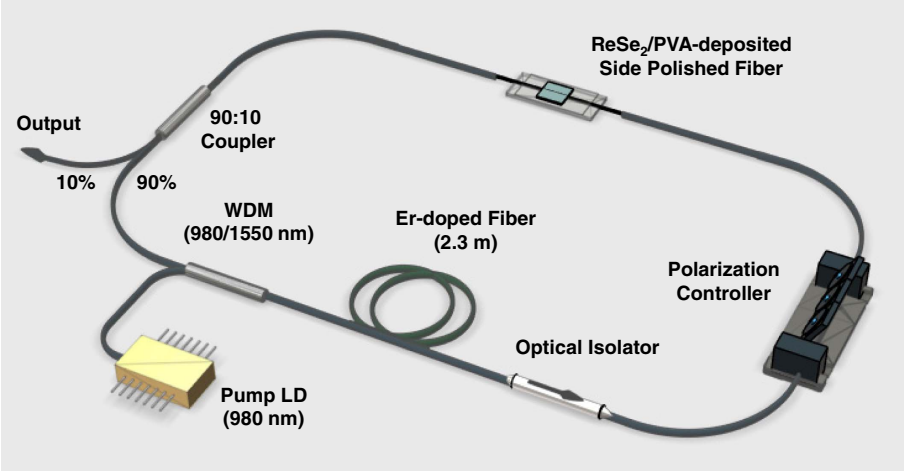

Fig. 8. Experimental configuration of our mode-locked fiber laser.

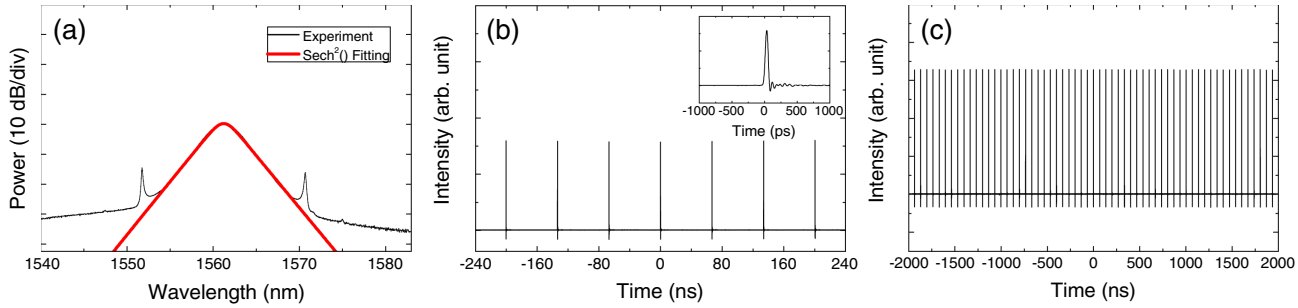

Fig. 9. (a) Optical spectrum and (b) an oscilloscope trace of the output pulses. Inset: oscilloscope trace for a narrow span. (c) An oscilloscope trace of the output pulses over a large time scale.

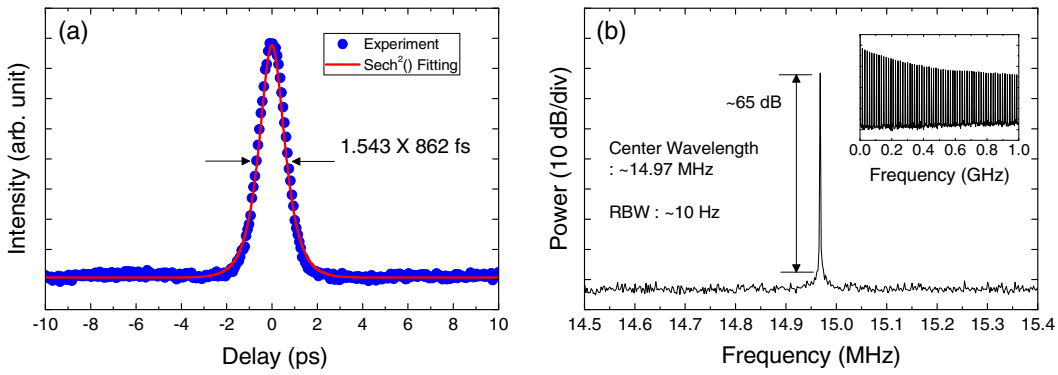

Fig. 10. (a) Autocorrelation trace and (b) electrical spectrum of the output pulses. Inset: electrical spectrum for a span of 1 GHz.

significantly vary depending on the SA sample change. It should be noticed that the mode-locking performance of a fiber laser with net anomalous cavity dispersion is not so dependent on the SA performance if the minimum parameter conditions of the SA used in the laser cavity such as modulation depth and saturation energy are satisfied [81]. We have also checked the long-term stability of the mode-locked fiber laser by observing the variation of the output pulses for several hours and did not find any substantial variations of the output pulses.

Finally, the output performance of our mode-locked fiber laser was compared to those of mode-locked fiber lasers using SAs based on other types of nonlinear optical materials. The results are summarized in Table 2. Our fabricated $ReSe_2$/PVA-based SA exhibited a modulation depth (~3.9%)

Table 2. Performance Comparison between the Present Work and Previously Demonstrated Mode-Locked Erbium-Doped Fiber Lasers Incorporating Other Saturable Absorption Materials

Saturable Absorption Materials	SA Threshold Level	Modulation Depth (%)	Wavelength (nm)	3 dB Bandwidth (nm)	Repetition Rate (MHz)	Pulse Width (ps)	Reference
CNT	NA[a]	NA	1556.2	3.7	5.88	0.47	[14]
Graphene	NA	NA	1559	5.24	19.9	0.464	[16]
Graphene	NA	NA	1561.6	1.96	6.99	1.3	[17]
GO	53 W[b]	5.25	1556.5	8.5	17.09	0.615	[19]
Bi_2Te_3	44 W	15.7	1547	4.63	15.11	0.6	[22]
Bi_2Se_3	12 MW/cm^2[c]	3.9	1557.5	4.3	12.5	0.66	[23]
Sb_2Te_3	NA	NA	1558.6	1.8	4.75	1.8	[24]
MoS_2	137 MW/cm^2	2.7	1556.3	6.1	463	0.935	[26]
WS_2	600 MW/cm^2	0.95	1557	2.3	8.86	1.32	[8]
$MoSe_2$	24 W	5.4	1555.6	5.4	15.38	0.798	[28]
WSe_2	NA	0.5	1557.6	2.1	5.31	1.25	[30]
$MoTe_2$	NA	1.8	1561	2.4	5.26	1.2	[31]
WTe_2	64.6 W	2.85	1556.2	4.14	13.98	0.77	[32]
SnS_2	125 MW/cm^2	4.6	1562.01	6.09	29.33	0.623	[33]
ReS_2	74 MW/cm^2	0.12	1558.6	1.85	5.4801	1.6	[37]
BP	6.55 MW/cm^2	8.1	1571.45	2.9	5.96	0.946	[46]
Gold nanorod	NA	4.9	1552	3.07	4.762	0.887	[49]
$CoSb_3$	8.7 W	5	1557.9	3.44	22.26	0.73	[52]
Ti_3CN	45 W	1.7	1557	5	15.4	0.66	[53]
$ReSe_2$	42 W	3.9	1561.2	3.4	14.97	0.862	This work

[a]NA, not available.
[b]Saturation power.
[c]Saturation intensity.

that is similar to systems based on GO, Bi_2Se_3, $MoSe_2$, SnS_2, gold nanorods, and $CoSb_3$. In terms of the pulse width of the output pulses, our fiber laser exhibits a reasonable level of the output pulse width (862 fs) for femtosecond laser applications. In terms of saturable absorption properties, $ReSe_2$ does not exhibit noticeable advantages over other nanomaterials. However, it should be noticed that the $ReSe_2$ particles used in this work are bulk-structured but not nanostructured. Their sizes were observed to vary from tens of nanometers to around 2 μm. Since bulk-structured materials do not require a complicated fabrication process, we believe that they have significant advantages over nanostructured ones in terms of ease of sample preparation.

6. CONCLUSION

We have systematically investigated the nonlinear optical properties of $ReSe_2$. The nonlinear absorption coefficient and the nonlinear refractive index of $ReSe_2$ were measured to be $-(5.67 \pm 0.35) \times 10^3$ cm/GW and $-(2.81 \pm 0.13) \times 10^{-2}$ cm^2/GW, respectively, using the OA and CA Z-scan technique at a wavelength of 1560 nm. The prepared $ReSe_2$ sample was shown to possess nonlinear saturable absorption and self-defocusing properties. The values of the nonlinear absorption coefficient and the nonlinear refractive index of $ReSe_2$ are comparable to those of other TMDC materials, as reported in previous studies. A fiberized SA was also fabricated using a side-polished-fiber platform by depositing a $ReSe_2$/PVA composite. Using the fabricated $ReSe_2$/PVA-based SA, stable mode-locked pulses with a temporal width of ~862 fs could be readily obtained from an EDF laser.

Further investigations for the improvement of the uniformity of the prepared $ReSe_2$ film are required to enhance the repeatability of the $ReSe_2$-based SA fabrication process. We believe that the results of this investigation confirm that $ReSe_2$ is a good candidate for the development of nonlinear optic or photonic devices.

Funding. National Research Foundation of Korea (NRF) (2018R1A2B6001641); Institute for Information and Communications Technology Planning & Evaluation (IITP) (IITP-2019-2015-0-00385).

REFERENCES

1. D.-S. Tsai, K.-K. Liu, D.-H. Lien, M.-L. Tsai, C.-F. Kang, C.-A. Lin, L.-J. Li, and J.-H. He, "Few-layer MoS_2 with high broadband photogain and fast optical switching for use in harsh environments," ACS Nano **7**, 3905–3911 (2013).
2. K. Wang, J. Wang, J. Fan, M. Lotya, A. O'Neill, D. Fox, Y. Feng, X. Zhang, B. Jiang, Q. Zhao, H. Zhang, J. N. Coleman, L. Zhang, and W. J. Blau, "Ultrafast saturable absorption of two-dimensional MoS_2 nanosheets," ACS Nano **7**, 9260–9267 (2013).
3. K. Wang, Y. Feng, C. Chang, J. Zhan, C. Wang, Q. Zhao, J. N. Coleman, L. Zhang, W. J. Blau, and J. Wang, "Broadband ultrafast nonlinear absorption and nonlinear refraction of layered molybdenum dichalcogenide semiconductors," Nanoscale **6**, 10530–10535 (2014).
4. S. H. Kassani, R. Khazaeinezhad, H. Jeong, T. Nazari, D.-I. Yeom, and K. Oh, "All-fiber Er-doped *Q*-switched laser based on tungsten disulfide saturable absorber," Opt. Mater. Express **5**, 373–379 (2015).
5. S. Wang, H. Yu, H. Zhang, A. Wang, M. Zhao, Y. Chen, L. Mei, and J. Wang, "Broadband few-layer MoS_2 saturable absorber," Adv. Mater. **26**, 3538–3544 (2014).
6. H. Zhang, S. B. Lu, J. Zheng, J. Du, S. C. Wen, D. Y. Tang, and K. P. Loh, "Molybdenum disulfide (MoS_2) as a broadband saturable absorber for ultra-fast photonics," Opt. Express **22**, 7249–7260 (2014).

7. X. Fu, J. Qian, X. Qiao, P. Tan, and Z. Peng, "Nonlinear saturable absorption of vertically stood WS_2 nanoplates," Opt. Lett. **39**, 6450–6453 (2014).
8. D. Mao, Y. Wang, C. Ma, L. Han, B. Jiang, X. Gan, S. Hua, W. Zhang, T. Mei, and J. Zhao, "WS_2 mode-locked ultrafast fiber laser," Sci. Rep. **5**, 7965 (2015).
9. K. P. Loh, H. Zhang, W. Z. Chen, and W. Ji, "Templated deposition of MoS_2 nanotubules using single source precursor and studies of their optical limiting properties," J. Phys. Chem. B **110**, 1235–1239 (2006).
10. E. Hendry, P. J. Hale, J. Moger, A. K. Savchenko, and S. A. Mikhailov, "Coherent nonlinear optical response of graphene," Phy. Rev. Lett. **105**, 097401 (2010).
11. G. Wang, S. Zhang, X. Zhang, L. Zhang, Y. Cheng, D. Fox, H. Zhang, J. N. Coleman, W. J. Blau, and J. Wang, "Tunable nonlinear refractive index of two-dimensional MoS_2, WS_2, and $MoSe_2$ nanosheet dispersions [Invited]," Photon. Res. **3**, A51–A55 (2015).
12. S. J. Varma, J. Kumar, Y. Li, K. Layne, J. Wu, C. Liang, Y. Nakanishi, A. Aliyan, W. Yang, P. M. Ajayan, and J. Thomas, "2D TiS_2 layers: a superior nonlinear optical limiting material," Adv. Opt. Mater. **5**, 1700713 (2017).
13. S. Y. Set, H. Yaguchi, Y. Tanaka, and M. Jablonski, "Laser mode locking using a saturable absorber incorporating carbon nanotubes," J. Lightwave Technol. **22**, 51–56 (2004).
14. Y.-W. Song, S. Yamashita, C. S. Goh, and S. Y. Set, "Carbon nanotube mode lockers with enhanced nonlinearity via evanescent field interaction in D-shaped fibers," Opt. Lett. **32**, 148–150 (2007).
15. Q. Bao, H. Zhang, Y. Wang, Z. Ni, Y. Yang, Z. X. Shen, K. P. Loh, and D. Y. Tang, "Atomic-layer graphene as a saturable absorber for ultrafast pulsed lasers," Adv. Funct. Mater. **19**, 3077–3083 (2009).
16. Z. Sun, T. Hasan, F. Torrisi, D. Popa, G. Privitera, F. Wang, F. Bonaccorso, D. M. Basko, and A. C. Ferrari, "Graphene mode-locked ultrafast laser," ACS Nano **4**, 803–810 (2010).
17. Y.-W. Song, S.-Y. Jang, W.-S. Han, and M.-K. Bae, "Graphene mode-lockers for fiber lasers functioned with evanescent field interaction," Appl. Phys. Lett. **96**, 051122 (2010).
18. K. P. Loh, Q. Bao, G. Eda, and M. Chhowalla, "Graphene oxide as a chemically tunable platform for optical applications," Nat. Chem. **2**, 1015–1024 (2010).
19. S. Ko, J. Lee, J. Koo, B. S. Joo, M. Gu, and J. H. Lee, "Chemical wet etching of an optical fiber using a hydrogen fluoride-free solution for a saturable absorber based on the evanescent field interaction," J. Lightwave Technol. **34**, 3776–3784 (2016).
20. F. Bernard, H. Zhang, S. P. Gorza, and P. Emplit, "Towards mode-locked fiber laser using topological insulators," in *Nonlinear Photonics*, OSA Technical Digest (online) (Optical Society of America, 2012), paper NTh1A.5.
21. Y. Chen, C. Zhao, H. Huang, S. Chen, P. Tang, Z. Wang, S. Lu, H. Zhang, S. Wen, and D. Tang, "Self-assembled topological insulator: Bi_2Se_3 membrane as a passive *Q*-switcher in an erbium-doped fiber laser," J. Lightwave Technol. **31**, 2857–2863 (2013).
22. J. Lee, J. Koo, Y. M. Jhon, and J. H. Lee, "A femtosecond pulse erbium fiber laser incorporating a saturable absorber based on bulk-structured Bi_2Te_3 topological insulator," Opt. Express **22**, 6165–6173 (2014).
23. H. Liu, X.-W. Zheng, M. Liu, N. Zhao, A.-P. Luo, Z.-C. Luo, W.-C. Xu, H. Zhang, C.-J. Zhao, and S.-C. Wen, "Femtosecond pulse generation from a topological insulator mode-locked fiber laser," Opt. Express **22**, 6868–6873 (2014).
24. J. Sotor, G. Sobon, W. Macherzynski, P. Paletko, K. Grodecki, and K. M. Abramski, "Mode-locking in Er-doped fiber laser based on mechanically exfoliated Sb_2Te_3 saturable absorber," Opt. Mater. Express **4**, 1–6 (2014).
25. Y. I. Jhon, J. Lee, Y. M. Jhon, and J. H. Lee, "Topological insulators for mode-locking of 2-μm fiber lasers," IEEE J. Sel. Top. Quantum Electron. **24**, 1102208 (2018).
26. K. Wu, X. Zhang, J. Wang, and J. Chen, "463-MHz fundamental mode-locked fiber laser based on few-layer MoS_2 saturable absorber," Opt. Lett. **40**, 1374–1377 (2015).
27. R. I. Woodward, E. J. R. Kelleher, R. C. T. Howe, G. Hu, F. Torrisi, T. Hasan, S. V. Popov, and J. R. Taylor, "Tunable *Q*-switched fiber laser based on saturable edge-state absorption in few-layer molybdenum disulfide (MoS_2)," Opt. Express **22**, 31113–31122 (2014).
28. J. Koo, J. Park, J. Lee, Y. M. Jhon, and J. H. Lee, "Femtosecond harmonic mode-locking of a fiber laser at 3.27 GHz using a bulk-like, $MoSe_2$-based saturable absorber," Opt. Express **24**, 10575–10589 (2016).
29. J. Lee, J. Koo, J. Lee, Y. M. Jhon, and J. H. Lee, "All-fiberized, femtosecond laser at 1912 nm using a bulk-like $MoSe_2$ saturable absorber," Opt. Mater. Express **7**, 2968–2979 (2017).
30. D. Mao, X. She, B. Du, D. Yang, W. Zhang, K. Song, X. Cui, B. Jiang, T. Peng, and J. Zhao, "Erbium-doped fiber laser passively mode locked with few-layer $WSe_2/MoSe_2$ nanosheets," Sci. Rep. **6**, 23583 (2016).
31. D. Mao, B. Du, D. Yang, S. Zhang, Y. Wang, W. Zhang, X. She, H. Cheng, H. Zeng, and J. Zhao, "Nonlinear saturable absorption of liquid-exfoliated molybdenum/tungsten ditelluride nanosheets," Small **12**, 1489–1497 (2016).
32. J. Koo, Y. I. Jhon, J. Park, J. Lee, Y. M. Jhon, and J. H. Lee, "Near-infrared saturable absorption of defective bulk-structured WTe_2 for femtosecond laser mode-locking," Adv. Funct. Mater. **26**, 7454–7461 (2016).
33. K. Niu, R. Sun, Q. Chen, B. Man, and H. Zhang, "Passively mode-locked Er-doped fiber laser based on SnS_2 nanosheets as a saturable absorber," Photon. Res. **6**, 72–76 (2018).
34. Y. Cui, F. Lu, and X. Liu, "Nonlinear saturable and polarization induced absorption of rhenium disulfide," Sci. Rep. **7**, 40080 (2017).
35. F. Lu, "Passively harmonic mode-locked fiber laser based on ReS_2 saturable absorber," Mod. Phys. Lett. B **31**, 1750206 (2017).
36. X. Su, H. Nie, Y. Wang, G. Li, B. Yan, B. Zhang, K. Yang, and J. He, "Few-layered ReS_2 as saturable absorber for 2.8 μm solid state laser," Opt. Lett. **42**, 3502–3505 (2017).
37. D. Mao, X. Cui, X. Gan, M. Li, W. Zhang, H. Lu, and J. Zhao, "Passively *Q*-switched and mode-locked fiber laser based on an ReS_2 saturable absorber," IEEE J. Sel. Top. Quantum Electron. **24**, 1100406 (2018).
38. X. Xu, M. Jiang, D. Li, R. Wang, Z. Ren, and J. Bai, "Passive Q-switching based on ReS_2 saturable absorber in Er-doped fiber laser at 1532 nm," Opt. Quantum Electron. **50**, 39 (2018).
39. L. Du, G. Jiang, L. Miao, B. Huang, J. Yi, C. Zhao, and S. Wen, "Few-layer rhenium diselenide: an ambient-stable nonlinear optical modulator," Opt. Mater. Express **8**, 926–935 (2018).
40. Z. Li, N. Dong, Y. Zhang, J. Wang, H. Yu, and F. Chen, "Invited article: mode-locked waveguide lasers modulated by rhenium diselenide as a new saturable absorber," APL Photon. **3**, 080802 (2018).
41. C. Li, Y. Leng, and J. Huo, "Diode-pumped solid-state *Q*-switched laser with rhenium diselenide as saturable absorber," Appl. Sci. **8**, 1753 (2018).
42. C. Li, Y. Leng, and J. Huo, "$ReSe_2$ as a saturable absorber in a Tm-doped yttrium lithium fluoride (Tm:YLF) pulse laser," Chin. Opt. Lett. **17**, 011402 (2019).
43. J. Wang, Z. Jiang, H. Chen, J. Li, J. Yin, J. Wang, T. He, P. Yan, and S. Ruan, "High energy soliton pulse generation by a magnetron-sputtering-deposition-grown $MoTe_2$ saturable absorber," Photon. Res. **6**, 535–541 (2018).
44. J. Wang, H. Chen, Z. Jiang, J. Yin, J. Wang, M. Zhang, T. He, J. Li, P. Yan, and S. Ruan, "Mode-locked thulium-doped fiber laser with chemical vapor deposited molybdenum ditelluride," Opt. Lett. **43**, 1998–2001 (2018).
45. J. Wang, Z. Jiang, H. Chen, J. Li, J. Yin, J. Wang, T. He, P. Yan, and S. Ruan, "Magnetron-sputtering deposited WTe_2 for an ultrafast thulium-doped fiber laser," Opt. Lett. **42**, 5010–5013 (2017).
46. Y. Chen, G. Jiang, S. Chen, Z. Guo, X. Yu, C. Zhao, H. Zhang, Q. Bao, S. Wen, D. Tang, and D. Fan, "Mechanically exfoliated black phosphorus as a new saturable absorber for both *Q*-switching and mode-locking laser operation," Opt. Express **23**, 12823–12833 (2015).
47. K. Park, J. Lee, Y. T. Lee, W.-K. Choi, J. H. Lee, and Y.-W. Song, "Black phosphorus saturable absorber for ultrafast mode-locked pulse laser via evanescent field interaction," Ann. Phys. **527**, 770–776 (2015).
48. S. B. Lu, L. L. Miao, Z. N. Guo, X. Qi, C. J. Zhao, H. Zhang, S. C. Wen, D. Y. Tang, and D. Y. Fan, "Broadband nonlinear optical response in

multi-layer black phosphorus: an emerging infrared and mid-infrared optical material," Opt. Express **23**, 11183–11194 (2015).
49. X.-D. Wang, Z.-C. Luo, H. Liu, M. Liu, A.-P. Luo, and W.-C. Xu, "Microfiber-based gold nanorods as saturable absorber for femtosecond pulse generation in a fiber laser," Appl. Phys. Lett. **105**, 161107 (2014).
50. D. Fan, C. Mou, X. Bai, S. Wang, N. Chen, and X. Zeng, "Passively *Q*-switched erbium-doped fiber laser using evanescent field interaction with gold-nanosphere based saturable absorber," Opt. Express **22**, 18537–18542 (2014).
51. J. Lee, B.-K. Yu, Y. I. Jhon, J. Koo, S. J. Kim, Y. M. Jhon, and J. H. Lee, "Filled skutterudites for broadband saturable absorbers," Adv. Opt. Mater. **5**, 1700096 (2017).
52. J. Lee, Y. Kim, K. Lee, and J. H. Lee, "Femtosecond mode-locking of a fiber laser using a $CoSb_3$-skutterudite-based saturable absorber [Invited]," Photon. Res. **6**, C36–C43 (2018).
53. Y. I. Jhon, J. Koo, B. Anasori, M. Seo, J. H. Lee, Y. Gogotsi, and Y. M. Jhon, "Metallic MXene saturable absorber for femtosecond mode-locked lasers," Adv. Mater. **29**, 1702496 (2017).
54. X. Jiang, S. Liu, W. Liang, S. Luo, Z. He, Y. Ge, H. Wang, R. Cao, F. Zhang, Q. Wen, J. Li, Q. Bao, D. Fan, and H. Zhang, "Broadband nonlinear photonics in few-layer MXene $Ti_3C_2T_x$ (T=F, O, or OH)," Laser Photon. Rev. **12**, 1700229 (2018).
55. Y. I. Jhon, J. Lee, M. Seo, J. H. Lee, and Y. M. Jhon, "van der Waals layered tin selenide as highly nonlinear ultrafast saturable absorber," Adv. Opt. Mater. **7**, 1801745 (2019).
56. Q. H. Wang, K. Kalantar-Zadeh, A. Kis, J. N. Coleman, and M. S. Strano, "Electronics and optoelectronics of two-dimensional transition metal dichalcogenides," Nat. Nanotechnol. **7**, 699–712 (2012).
57. S. Zhang, N. Dong, N. McEvoy, M. O'Brien, S. Winters, N. C. Berner, C. Yim, Y. Li, X. Zhang, Z. Chen, L. Zhang, G. S. Duesberg, and J. Wang, "Direct observation of degenerate two-photon absorption and its saturation in WS_2 and MoS_2 monolayer and few-layer films," ACS Nano **9**, 7142–7150 (2015).
58. R. I. Woodward, R. T. Murray, C. F. Phelan, R. E. P. de Oliveira, T. H. Runcorn, E. J. R. Kelleher, S. Li, E. C. de Oliveira, G. J. M. Fechine, G. Eda, and C. J. S. de Matos, "Characterization of the second- and third-order nonlinear optical susceptibilities of monolayer MoS_2 using multiphoton microscopy," 2D Mater. **4**, 011006 (2017).
59. N. Kumar, S. Najmaei, Q. Cui, F. Ceballos, P. M. Ajayan, J. Lou, and H. Zhao, "Second harmonic microscopy of monolayer MoS_2," Phys. Rev. B **87**, 161403 (2013).
60. R. Wang, H.-C. Chien, J. Kumar, N. Kumar, H.-Y. Chiu, and H. Zhao, "Third-harmonic generation in ultrathin films of MoS_2," ACS Appl. Mater. Interfaces **6**, 314–318 (2014).
61. S. Yang, C. Wang, H. Sahin, H. Chen, Y. Li, S.-S. Li, A. Suslu, F. M. Peeters, Q. Liu, J. Li, and S. Tongay, "Tuning the optical, magnetic, and electrical properties of $ReSe_2$ by nanoscale strain engineering," Nano Lett. **15**, 1660–1666 (2015).
62. H. Zhao, J. Wu, H. Zhong, Q. Guo, X. Wang, F. Xia, L. Yang, P. Tan, and H. Wang, "Interlayer interactions in anisotropic atomically thin rhenium diselenide," Nano Res. **8**, 3651–3661 (2015).
63. H. Yang, H. Jussila, A. Autere, H.-P. Komsa, G. Ye, X. Chen, T. Hasan, and Z. Sun, "Optical waveplates based on birefringence of anisotropic two-dimensional layered materials," ACS Photon. **4**, 3023–3030 (2017).
64. C. M. Corbet, S. S. Sonde, E. Tutuc, and S. K. Banerjee, "Improved contact resistance in $ReSe_2$ thin film field-effect transistors," Appl. Phys. Lett. **108**, 162104 (2016).
65. F. Qi, X. Wang, B. Zheng, Y. Chen, B. Yu, J. Zhou, J. He, P. Li, W. Zhang, and Y. Li, "Self-assembled chrysanthemum-like microspheres constructed by few-layer $ReSe_2$ nanosheets as a highly efficient and stable electrocatalyst for hydrogen evolution reaction," Electrochim. Acta **224**, 593–599 (2017).
66. P. Hu, M. Jia, Y. Zuo, and L. He, "A silica/PVA adhesive hybrid material with high transparency, thermostability and mechanical strength," RSC Adv. **7**, 2450–2459 (2017).
67. X. Zhang, Y. Zhou, and J. Zhang, "In-situ reduced graphene oxide-polyvinyl alcohol composite coatings as protective layers on magnesium substrates," Prog. Nat. Sci. **27**, 326–328 (2017).
68. D. Wolverson, S. Crampin, A. S. Kazemi, A. Ilie, and S. J. Bending, "Raman spectra of monolayer, few-layer, and bulk $ReSe_2$: an anisotropic layered semiconductor," ACS Nano **8**, 11154–11164 (2014).
69. S. Jiang, Z. Zhang, N. Zhang, Y. Huan, Y. Gong, M. Sun, J. Shi, C. Xie, P. Yang, Q. Fang, H. Li, L. Tong, D. Xie, L. Gu, P. Liu, and Y. Zhang, "Application of chemical vapor-deposited monolayer $ReSe_2$ in the electrocatalytic hydrogen evolution reaction," Nano Res. **11**, 1787–1797 (2018).
70. S. Yang, S. Tongay, Y. Li, Q. Yue, J.-B. Xia, S.-S. Li, J. Li, and S.-H. Wei, "Layer-dependent electrical and optoelectronic responses of $ReSe_2$ nanosheet transistors," Nanoscale **6**, 7226–7231 (2014).
71. H.-X. Zhong, S. Gao, J.-J. Shi, and L. Yang, "Quasiparticle band gaps, excitonic effects, and anisotropic optical properties of the monolayer distorted 1T diamond-chain structures ReS_2 and $ReSe_2$," Phys. Rev. B **92**, 115438 (2015).
72. R. I. Woodward and E. J. R. Kelleher, "2D saturable absorber for fibre lasers," Appl. Sci. **5**, 1440–1456 (2015).
73. M. Sheik-Bahae, A. A. Said, and E. W. Van Stryland, "High-sensitivity, single-beam n_2 measurements," Opt. Lett. **14**, 955–957 (1989).
74. Y. Ge, Z. Zhu, Y. Xu, Y. Chen, S. Chen, Z. Liang, Y. Song, Y. Zou, H. Zeng, S. Xu, H. Zhang, and D. Fan, "Broadband nonlinear photoresponse of 2D TiS_2 for ultrashort pulse generation and all-optical thresholding devices," Adv. Opt. Mater. **6**, 1701166 (2018).
75. X. Jiang, L. Zhang, S. Liu, Y. Zhang, Z. He, W. Li, F. Zhang, Y. Shi, W. Lü, Y. Li, Q. Wen, J. Li, J. Feng, S. Ruan, Y.-J. Zeng, X. Zhu, Y. Lu, and H. Zhang, "Ultrathin metal-organic framework: an emerging broadband nonlinear optical material for ultrafast photonics," Adv. Opt. Mater. **6**, 1800561 (2018).
76. M. Zhang, R. C. T. Howe, R. I. Woodward, E. J. R. Kelleher, F. Torrisi, G. Hu, S. V. Popov, J. R. Taylor, and T. Hasan, "Solution processed MoS_2-PVA composite for sub-bandgap mode-locking of a wideband tunable ultrafast Er:fiber laser," Nano Res. **8**, 1522–1534 (2015).
77. M. Zhang, G. Hu, G. Hu, R. C. T. Howe, L. Chen, Z. Zheng, and T. Hasan, "Yb- and Er-doped fiber laser *Q*-switched with an optically uniform, broadband WS_2 saturable absorber," Sci. Rep. **5**, 17482 (2015).
78. X. Zheng, Y. Zhang, R. Chen, X. Cheng, Z. Xu, and T. Jiang, "Z-scan measurement of the nonlinear refractive index of monolayer WS_2," Opt. Express **23**, 15616–15623 (2015).
79. S. Bikorimana, P. Lama, A. Walser, R. Dorsinville, S. Anghel, A. Mitioglu, A. Micu, and L. Kulyuk, "Nonlinear optical responses in two-dimensional transition metal dichalcogenide multilayer: WS_2, WSe_2, MoS_2 and $Mo_{0.5}W_{0.5}S_2$," Opt. Express **24**, 20685–20695 (2016).
80. C. Hönninger, R. Paschotta, F. Morier-Genoud, M. Moser, and U. Keller, "*Q*-switching stability limits of continuous-wave passive mode locking," J. Opt. Soc. Am. B **16**, 46–56 (1999).
81. J. Jeon, J. Lee, and J. H. Lee, "Numerical study on the minimum modulation depth of a saturable absorber for stable fiber laser mode locking," J. Opt. Soc. Am. B **32**, 31–37 (2015).
82. K. Wu, B. Chen, X. Zhang, S. Zhang, C. Guo, C. Li, P. Xiao, J. Wang, L. Zhou, W. Zou, and J. Chen, "High-performance mode-locked and *Q*-switched fiber lasers based on novel 2D materials of topological insulators, transition metal dichalcogenides and black phosphorus: review and perspective (invited)," Opt. Commun. **406**, 214–229 (2018).
83. S. M. J. Kelly, "Characteristic sideband instability of periodically amplified average soliton," Electron. Lett. **28**, 806–807 (1992).